

Van der Waals Electrides

Published as part of Accounts of Chemical Research special issue "2D Materials".

Jun Zhou, Jing-Yang You, Yi-Ming Zhao, Yuan Ping Feng, and Lei Shen*



Cite This: *Acc. Chem. Res.* 2024, 57, 2572–2581



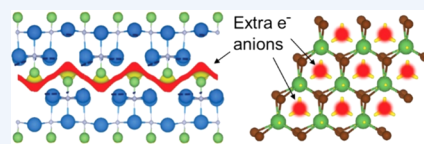
Read Online

ACCESS |

Metrics & More

Article Recommendations

CONSPECTUS: Electrides make up a fascinating group of materials with unique physical and chemical properties. In these materials, excess electrons do not behave like normal electrons in metals or form any chemical bonds with atoms. Instead, they "float" freely in the gaps within the material's structure, acting like negatively charged particles called anions (see the graph). Recently, there has been a surge of interest in van der Waals (vdW) electrides or electrenes in two dimensions. A typical example is layered lanthanum bromide (LaBr_2), which can be taken as $[\text{La}^{3+}(\text{Br}^{-})_2]^{+}\bullet(\text{e}^{-})$. Each excess free electron is trapped within a hexagonal pore, forming dense dots of electron density. These anionic electrons are loosely bound, giving vdW electrides some unique properties such as ferromagnetism, superconductivity, topological features, and Dirac plasmons. The high density of the free electron makes electrides very promising for applications in thermionic emission, organic light-emitting diodes, and high-performance catalysts.



In this Account, we first discuss the discovery of numerous vdW electrides through high-throughput computational screening of over 67,000 known inorganic crystals in Materials Project. A dozen of them have been newly discovered and have not been reported before. Importantly, they possess completely different structural prototypes and properties of anionic electrons compared to widely studied electrides such as Ca_2N . Finding these new vdW electrides expands the variety of electrides that can be made in the experiment and opens up new possibilities for studying their unique properties and applications.

Then, based on the screened vdW electrides, we delve into their various emerging properties. For example, we developed a new magnetic mechanism specific to atomic-orbital-free ferromagnetism in electrides. We uncover the dual localized and extended nature of the anionic electrons in such electrides and demonstrate the formation of the local moment by the localized feature and the ferromagnetic interaction by the direct overlapping of their extended states. We further show the effective tuning of the magnetic properties of vdW electrides by engineering their structural, electronic, and compositional properties. Besides, we show that the complex interaction between the multiple quantum orderings in vdW electrides leads to many interesting properties including valley polarization, charge density waves, a topological property, a superconducting property, and a thermoelectrical property.

Moreover, we discuss strategies to leverage the unique intrinsic properties of vdW electrides for practical applications. We show that these properties make vdW electrides potential candidates for advanced applications such as spin-orbit torque memory devices, valleytronic devices, K-ion batteries, and thermoelectricity. Finally, we discuss the current challenges and future perspectives for research using these emerging materials.

KEY REFERENCES

- Zhou, J.; Shen, L.; Yang, M.; Cheng, H.; Kong, W.; Feng, Y. P. Discovery of Hidden Classes of Layered Electrides by Extensive High-Throughput Material Screening. *Chem. Mater.* **2019**, *31*(6), 1860–1868.¹ *This work identifies 24 vdW electrides through the high-throughput screening of Materials Project. These vdW electrides significantly increase the pool of experimentally synthesizable vdW electrides and provide a new material platform for exploring exotic properties and promising applications.*
- Zhou, J.; Feng, Y. P.; Shen, L. Atomic-orbital-free intrinsic ferromagnetism in electrenes. *Phys. Rev. B* **2020**, *102*(18), 180407(R).² *This work proposes that monolayer electrides, named electrenes, may be a new type of 2D*

intrinsic ferromagnetic material with unique atomic-orbital-free magnetism.

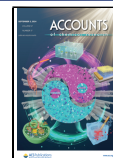
- Cheng, H.-X.; Zhou, J.; Ji, W.; Zhang, Y.-N.; Feng, Y.-P. Two-dimensional intrinsic ferrovalley GdI_2 with large valley polarization. *Phys. Rev. B* **2021**, *103*(12), 125121.³ *This work demonstrates ferrovalley and valley polarization in electrenes. Finally, an electrene-based valleytronic device is also proposed.*

Received: June 22, 2024

Revised: August 1, 2024

Accepted: August 6, 2024

Published: August 19, 2024



- You, J. Y.; Gu, B.; Su, G.; Feng, Y. P. Emergent Kagome Electrides. *J. Am. Chem. Soc.* **2022**, *144*(12), 5527–5534.⁴ This work develops a model to form a 2D Kagome lattice, coined 2D Kagome electrides, which have topological Dirac cones, flat bands, and superconductivity.

1. INTRODUCTION

Electrides are featured by anionic electrons (AEs), which reside at lattice interstitial spaces as anions.⁵ This concept evolved from earlier ideas about solvated electrons and color centers in solids.⁶ Later, aiming to crystallize alkali solutions to immobilize solvated electrons off-atom, the synthesis of the first single-crystal electride, a cesium crown-ether complex, was reported in 1982.⁷ Subsequently, various organic electrides with large pores were identified.^{8,9} However, their instability to air and moisture exposure due to vulnerable AEs and temperature sensitivity akin to that of molecular crystals have presented significant challenges. A significant breakthrough has been achieved with the synthesis of a thermally stable inorganic electride, where anions are safeguarded by a porous structure.¹⁰ Such a porous electride is formed by removing oxygen atoms from the crystallographic cages of $12\text{CaO}\cdot7\text{Al}_2\text{O}_3$, yielding $[\text{Ca}_{24}\text{Al}_{28}\text{O}_{64}]^{4+}(4\text{e}^-)$. Further research on the room-temperature stable porous electride has revealed that their intrinsic high density of loosely bound anions opens up various potential applications such as organic light-emitting diodes,¹¹ efficient thermionic emitters,¹² and high-performance catalysts.¹³

van der Waals (vdW) materials, including two-dimensional (2D) materials, their multilayers, and vdW heterostructures, have been attracting intense research interest due to their exceptional physical and chemical properties and a wide range of promising applications in flexible electronics, energy-related applications, and more.^{14,15} Electrides in vdW structures are particularly interesting because they may demonstrate new properties and serve as unique functional units that can be combined with other vdW materials. The first reported vdW electride is Ca_2N , in which excess electrons are confined between $[\text{Ca}_2\text{N}]^+$ layers, forming 2D electron layers.¹⁶ The experimental realization of monolayer Ca_2N highlights the potential for exfoliating vdW electrides into advanced 2D materials, called electrenes.¹⁷ Inspired by these developments, tens of new vdW electrides have been uncovered by high-throughput screening and global structure optimization methods.^{18–20} However, the current research on vdW electrides still mainly focuses on the nitrides and carbides within the structure prototype of Ca_2N . This motivated us to perform a thorough screening of the material database for vdW electrides.

In this Account, we summarize our recent progress in vdW electrides, focusing on the high-throughput screening process and covering various phenomena, including magnetic properties and quantum effects, as well as their applications to spin-orbit torque antiferromagnetic memory devices, valleytronic devices, K-ion batteries, and thermoelectricity. Finally, we discuss current challenges and future perspectives in the research of vdW electrides.

2. HIGH-THROUGHPUT SCREENING OF vdW ELECTRIDES

Given the inherent instability of electrides, theoretical designs face uncertainty regarding their experimental viability.²¹

Utilizing experimentally grown compounds from databases offers a more efficient method for identifying electrides. However, initial database screenings using Ca_2N as a template significantly limited the search scope to similar materials.^{19,20} To conduct a more unbiased screening, we focus on basic descriptors derived from the definition of electrides, including imbalanced total oxidation states and localized electrons in interstitial spaces.

We started from >67,000 inorganic compounds in the Materials Project (Figure 1a).²² A geometry-based algorithm

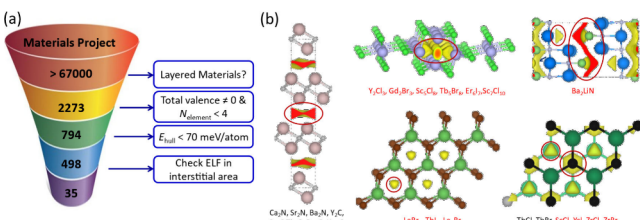


Figure 1. (a) Screening process for vdW electrides. (b) Screened electrides in different structure prototypes. The compositions in black are reported electrides, while those in red are new. The ELFs in the red circles are the AEs. Reproduced from ref 1. Copyright 2019 American Chemical Society.

identified potential layered materials, followed by a selection of binary and ternary compounds with imbalanced total oxidation states.²³ We use energy above hull ≤ 70 meV/atom to identify synthesizable electrides.²⁴ Notably, all newly screened electrides have been experimentally grown.²⁵ This screening yielded 498 candidates for high-throughput calculations. Electron localization functions (ELF) were computed to identify compounds with localized electrons in the interstitial area.^{18,19} Each candidate underwent further examination, including interstitial space size, projected density of states (PDOS) contribution, band decomposed charge density distribution, and a literature review of experimental results.

This screening process identified 24 vdW electrides, which were categorized into different structural prototypes (Figure 1b). Among them, 12 were previously reported, showcasing the reliability of our screening procedure.^{18,19} The remaining dozen compounds, highlighted in red in Figure 1b, were newly identified electrides. These vdW electrides exhibit diverse features, including fully spin-polarized zero-dimensional (0D) anionic electrons in metal halides, one-dimensional (1D) AEs confined within quasi-1D structures, the coexistence of 0D and 1D AEs in Ba_2LiN , and the coexistence of magnetic and nonmagnetic AEs found in ZrCl-like structures. This work significantly broadens the range of experimentally synthesizable vdW electrides and offers a platform for investigating their emergent properties.

3. EMERGING PROPERTIES OF vdW ELECTRIDES

vdW electrides represent a new class of materials with various emerging properties and potential applications for exploration. In this section, we present recent research elucidating their novel characteristics and their interaction with multiple quantum phenomena.

3.1. Unique Magnetic Properties and Engineering

3.1.1. Dual Localized and Extended Nature of Anionic Electrons. Research on 2D magnetism has surged since the fabrication of 2D ferromagnets in 2017.²⁶ However, they can

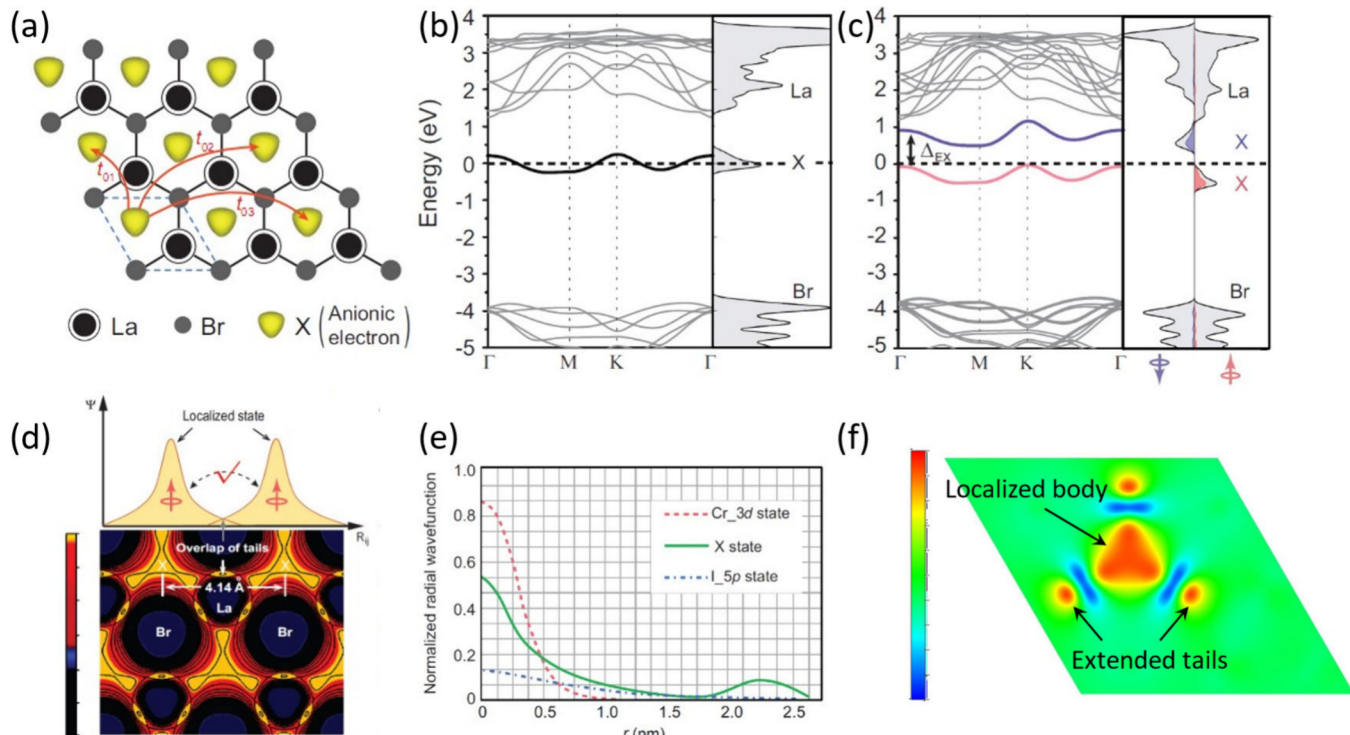


Figure 2. (a) H-phase LaBr_2 with ELF maps (isovalue = 0.75) in yellow. The red arrows denote the hopping paths between the AEs. Band structure and density of states of monolayer LaBr_2 (b) without and (c) with spin polarization. The yellow band and DOS in (b) are from the one-band model. (d) The calculated spin density of monolayer LaBr_2 (isovalue = $0.001 \text{ e}/\text{\AA}^3$). (e) Radial distributions of the normalized wave function of states of Cr_{3d} , I_{5p} , and AE. (f) The contour plot of the MLWF (isovalue = 2.0) of the AE of LaBr_2 colored in the plane passing through the La atoms. Reproduced with permission from ref 2. Copyright 2020 American Physical Society.

be explained by conventional theories developed for 3D materials, which emphasize the role of atomic orbitals in forming magnetic moments and exchange coupling through orbital hybridization. This contrasts with the atomic-orbital-free nature of AEs in electrides, necessitating a new understanding of magnetism in vdW electrides. With such motivation, we screened our 2D materials database—2DMatPedia—for magnetic electrides. Surprisingly, screened LaBr_2 , La_2Br_5 , $\text{Sc}_7\text{Cl}_{10}$, and Ba_2LiN do not have magnetic elements. It is noted that magnetic electrides in three dimensions may exhibit various states, such as ferromagnetism, antiferromagnetism, and interstitial magnetism.²⁷ However, in our work, we focus exclusively on interstitial magnetism, where anionic electrons act as magnetic centers.

Next, we use LaBr_2 as an example for a thorough physical investigation.² The AE, labeled as X, is at the center of each hexagon for LaBr_2 (Figure 2a). This state contributes a narrow band and a high density of states at the Fermi level (E_F) (Figure 2b). By Stoner criterion,²⁸ such high DOS is unstable and prefers spontaneous spin polarization. The spin-polarized simulation yields a local moment of $1 \mu_B/\text{u.c.}$ for LaBr_2 , (Figure 2c), which is mainly from the AEs by the projected DOS and spin density (Figure 2d). The comparison for the radial distributions of the wave functions of the AE, Cr_{3d} and I_{5p} orbitals in CrI_3 ,²⁶ shows that AE is localized as the d orbital and meanwhile is more extended than the p orbital. Based on this dual localized and extended nature of the AEs, we propose the formation of the local moment by the localized feature along with the ferromagnetic interaction between AEs by overlapping the extended AE states (Figure 2e).

A low-energy effective model based on the second quantization in terms of a maximally localized Wannier function (MLWF) was used to understand the underlying mechanism.²⁹ Notably, the interstitial-centered MLWFs captured the extended tails around the well-localized body (Figure 2f). The parameters mapped by the MLWF-based constrained random phase approximation (cRPA)³⁰ are $t_{01} = 12.50 \text{ meV}$, $U_{00} = 2.32 \text{ eV}$, $U_{01} = 1.36 \text{ eV}$, $J_{01}^D = 21.9 \text{ meV}$, and $J_{02}^D = 1.9 \text{ meV}$, where $i(j)$, t_{ij} , U_{00} , U_{ij} , and J_{ij}^D are site indexes, hopping parameters, on-site Coulomb, off-site Coulomb, and off-site direct-exchange interactions, respectively. Surprisingly, the direct exchange coupling between AEs remains significant over 7.17 \AA , which is beyond the spatial limit of atomic-orbital overlap in other direct-exchange systems. The large U_{00} and U_{01} are from weak screening from the atomic states because the AE state is well isolated from other bands. Moreover, the large off-site Coulomb interaction U_{01} suggests a large spatial charge fluctuation in LaBr_2 , in line with the extended nature of the AE. And the much larger effective Coulomb interaction $\tilde{U} = U_{00} - U_{01}$ compared to the hopping integral indicates the localized nature of the AEs. Considering $\tilde{U} \gg t_{01}$, Anderson's model is used to estimate the overall isotropic exchange interaction,³¹ which is -21.7 meV . This isotropic exchange surpasses the DFT-derived result (-6.5 meV) due to the latter's incapacity to accurately describe nonlocal direct-exchange interactions. This underscores the rationale behind opting for the low-energy effective model to unveil the underlying exchange mechanism of atomic-orbital-free intrinsic magnetism in vdW electrides.

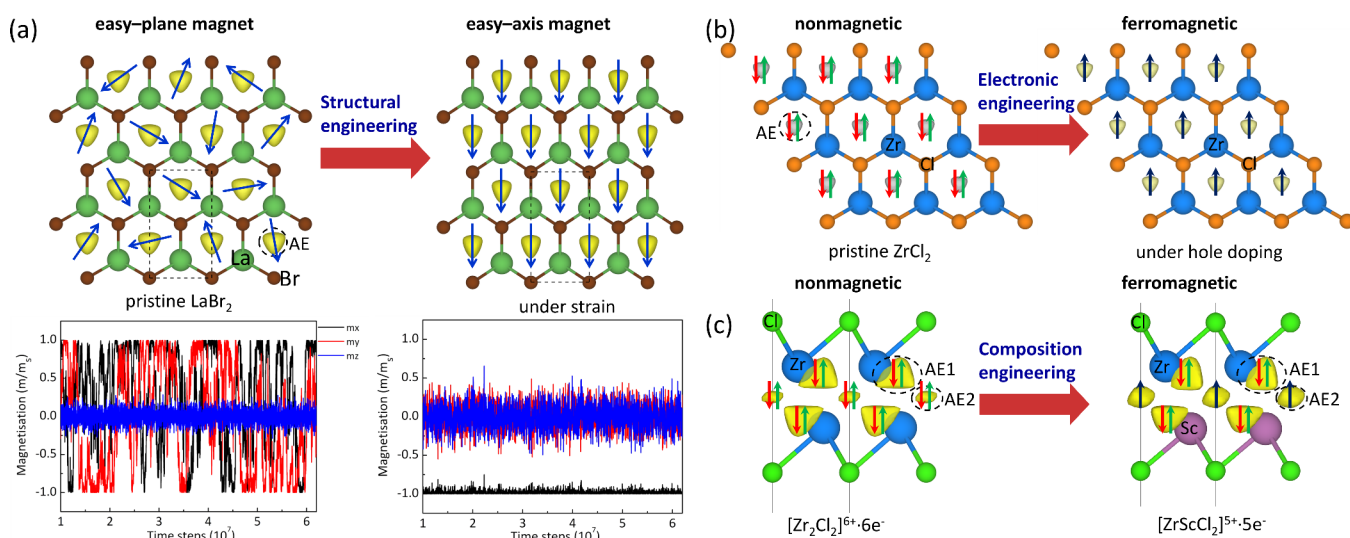


Figure 3. (a) Stabilizing long-range ferromagnetic ordering by structural engineering. The lower panel shows the Monte Carlo simulations for the evaluation of the projected averaged magnetism along [100] (m_x), [010] (m_y), and [001] (m_z) directions with times steps at 15 K for LaBr_2 under 0% (left), and +6% strains (right). Reproduced from ref 34. Copyright 2021 Royal Society of Chemistry. (b) Introducing magnetic AEs by electronic engineering of ZrCl_2 . Reproduced from ref 36. Copyright 2022 Royal Society of Chemistry. (c) Introducing magnetic AEs by composition engineering of ZrCl . Reproduced with permission from ref 38. Copyright 2023 Elsevier.

3.1.2. Stabilizing Long-Range Ferromagnetic Ordering by Strain Engineering. For long-range magnetic ordering at finite temperatures, magnetic anisotropy is required.³² Unfortunately, intrinsic LaBr_2 is an easy-plane magnet, in which the magnetic moments rotate randomly in the plane, preventing a collective magnetism (Figure 3a).³³ To induce the magnetic anisotropy, we propose applying in-plane uniaxial strains.³⁴ The total magnetic moment remains at $1 \mu_B/\text{f.u.}$, within the range of strain, implying the robustness of this material under strain. Importantly, the uniaxial strains induce a magnetically easy axis in LaBr_2 . For example, the 6% tensile strain along the [100] produces a magnetic easy axis with a magnetic anisotropy energy (MAE) of $E_{[010]} - E_{[100]} = 15 \mu\text{eV}/\text{f.u.}$.

Monte Carlo (MC) simulations show that the spins rotate randomly within the plane of pristine LaBr_2 (lower panel of Figure 3a). On the contrary, the spins are pinned along the [100] direction under 6% tensile strain, forming a collective ferromagnetic ordering. The temperature-dependent magnetization confirms the absence of long-range magnetic ordering in pristine LaBr_2 with collective ferromagnetism for up to 318 K under strain. These results provide direct evidence of the effectiveness of the uniaxial strain in tuning the magnetic anisotropy from an easy plane to an easy axis and correspondingly stabilizing the long-range magnetic ordering.

3.1.3. Inducing Ferromagnetism by Doping Engineering. Carrier doping is another effective engineering approach. This method is particularly suitable for 2D materials because conventional chemical doping in bulk materials suffers from low carrier density and technological limitations while gate-controlled electrostatic doping for 2D materials is reversible, nondestructive, has high carrier densities, and allows electrical control of magnetism.³⁵

Next, we use H-phase ZrCl_2 , a nonmagnetic semiconducting electride with two excess electrons per formula unit (f.u.), as an example by a series of hole doping concentrations of up to 1 hole/f.u. (Figure 3b).³⁶ A transition from the nonmagnetic to magnetic happened at around 0.5 hole/f.u.. The magnetic

moment increases with the hole doping concentration and reaches $1 \mu_B/\text{f.u.}$ at 1 hole/f.u., implying full spin polarization of the AE band. Our combined low-energy effective model, cRPA simulation, and Anderson's model further confirm the dual localized and extended nature of the hole-induced magnetic AEs in ZrCl_2 . Our results utilize the intrinsic properties of electrenes to introduce magnetism in nonmagnetic systems, paving the way for controllable novel spintronic applications.

3.1.4. Inducing Ferromagnetism by Composition Engineering. Conventional Janus materials consist of different same-column anions on the two sides.³⁷ Interestingly, electrides are electron-rich, which may accommodate the substitution of cations with smaller oxidation states. This enables us to propose a new type of Janus structure: electrides with cross-column cations on the two sides.³⁸ Here, we design nine Janus electrenes by substituting one zirconium atom layer of Zr_2Cl_2 with rare earth metal ($X^{\text{III}} = \text{Sc}, \text{Y}, \text{La}$), alkaline earth metal ($X^{\text{II}} = \text{Ca}, \text{Sr}, \text{Ba}$), or alkali metal ($X^{\text{I}} = \text{Na}, \text{K}, \text{Rb}$) cations. Phonon spectra confirm the dynamic stability of three Janus electrenes (ZrScCl_2 , ZrYCl_2 , and ZrCaCl_2).

Next, we use ZrScCl_2 as an example to illustrate the introduction of magnetism by forming a Janus structure. The simulated ELF shows three geometrical interstitial sites for AEs in ZrCl_2 (Figure 3c). While AE1 is at the center of the $\text{Zr}-\text{Cl}$ hexagons in each ZrCl sublayer, AE2 is at the center of the octahedrons of the six Zr ions. The ELFs in Figure 3c demonstrate a similar AE distribution of Janus ZrScCl_2 with ZrCl_2 . However, considering that Sc can provide one less electron than Zr, the AE1 state should not be fully occupied. From the band structure, the fully occupied spin-up channel and partially occupied spin-down channel of the AE1 produce a total magnetic moment of $0.52 \mu_B$ for ZrScCl_2 . The spin density of the magnetic Janus electride ZrScCl_2 confirms the spin-polarized AE1. The magnetic AEs are likely to possess a dual localized and extended nature.² Our results open up a new method to effectively tune the electronic and magnetic properties of electrenes.

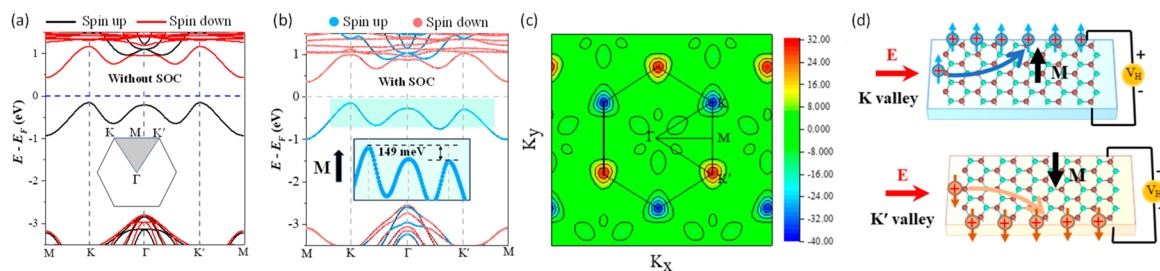


Figure 4. Band structure of GdI_2 (a) without SOC and (b) with SOC. (c) Berry curvature of GdI_2 on a contour map in the 2D Brillouin zone. (d) Schematic diagram of the tunable anomalous valley Hall effect in hole-doped GdI_2 in the K and K' valleys. “+” denotes the holes. Arrows in blue and brown refer to the spin-up and spin-down carriers, respectively. Reproduced with permission from ref 3. Copyright 2021 American Physical Society.

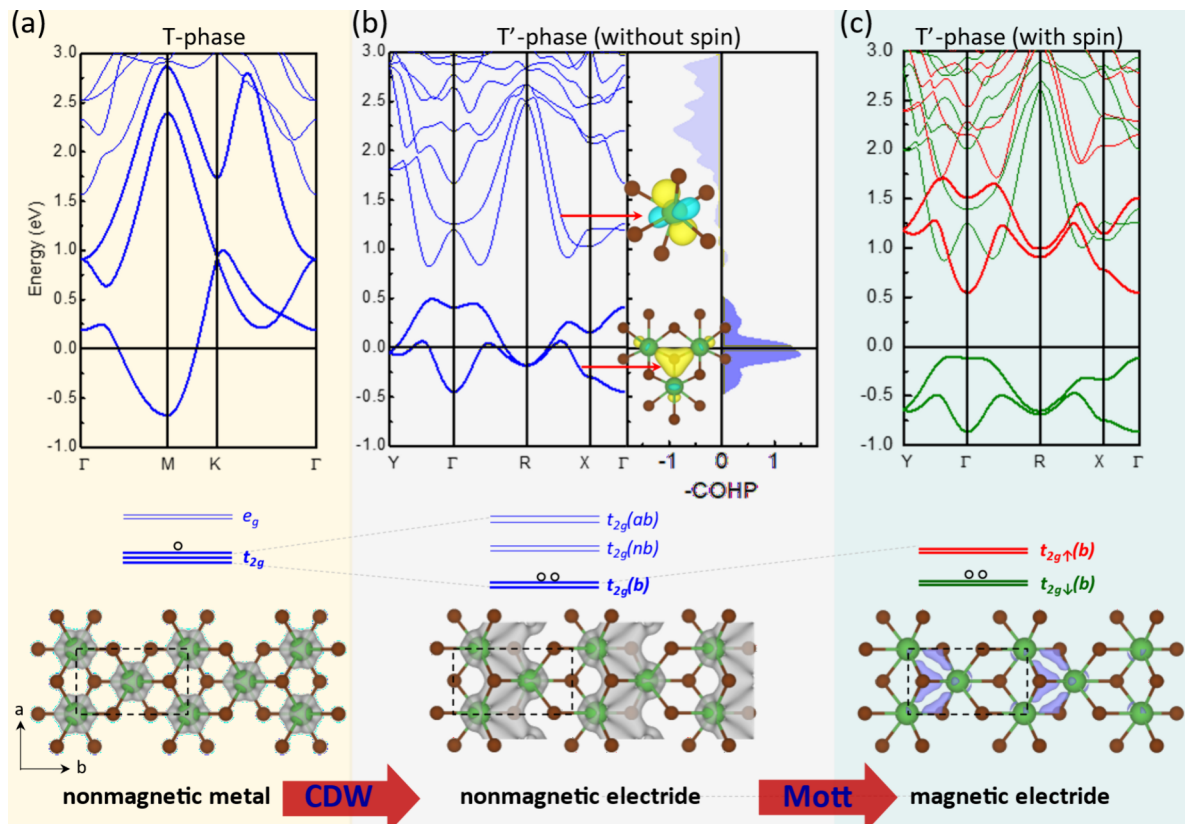


Figure 5. (a) Band structure and charge density of T LaBr_2 . (b) Band structure and $-\text{COHP}$ plots for the T' -phase LaBr_2 without spin polarization. The inset is the maximally localized Wannier function. It is noted that another two MLWFs similar to the inset are not shown. (c) Band structure of T' LaBr_2 with spin polarization. The red (green) lines represent the spin-up (spin-down) bands. The E_F is aligned to 0 eV. Reproduced from ref 45. Copyright 2023 Royal Society of Chemistry.

3.2. Interplay of Multiple Quantum Phenomena in vdW Electrodes

The multiple quantum phenomena in one system usually interplay with each other. For example, the charge density wave (CDW), which features real-space periodic lattice distortions and a reciprocal-space band gap opening, usually competes with magnetism.³⁹ This is because CDW gaps decrease the DOS at E_F , while the Stoner criterion requires the opposite. Therefore, their coexistence is rare.²⁸ However, such interactions may change in vdW electrodes.

3.2.1. Inducing Valley Polarization by Magnetization. Valley, a new degree of freedom alongside charge and spin, manifests as local energy extremes in a material's conduction or valence bands.⁴⁰ The practical applications of the recently proposed ferrovalley materials, characterized by intrinsic

spontaneous valley polarization,⁴¹ are hindered by the rare existence, small intrinsic valley splitting gaps, and low Curie temperatures. The quest for high Curie temperature ferrovalley materials with substantial valley polarization remains paramount for advancing next-generation electronics.

Considering the variety of rare-earth iodides and their similar structure with TMDs, we collected the experimentally reported rare-earth iodides⁴² for DFT simulations. An ideal ferrovalley material requires 1) the H phase as the ground state, 2) semiconducting properties, and 3) ferromagnetic properties. These criteria pinpoint three candidates: LaBr_2 , PrI_2 , and GdI_2 . Among them, GdI_2 has the largest valley splitting of 149 meV. Furthermore, the high Curie temperature (241 K) of monolayer GdI_2 ⁴³ ensures its practical applications. Thus, we focus on GdI_2 to dig into its ferrovalley properties.³

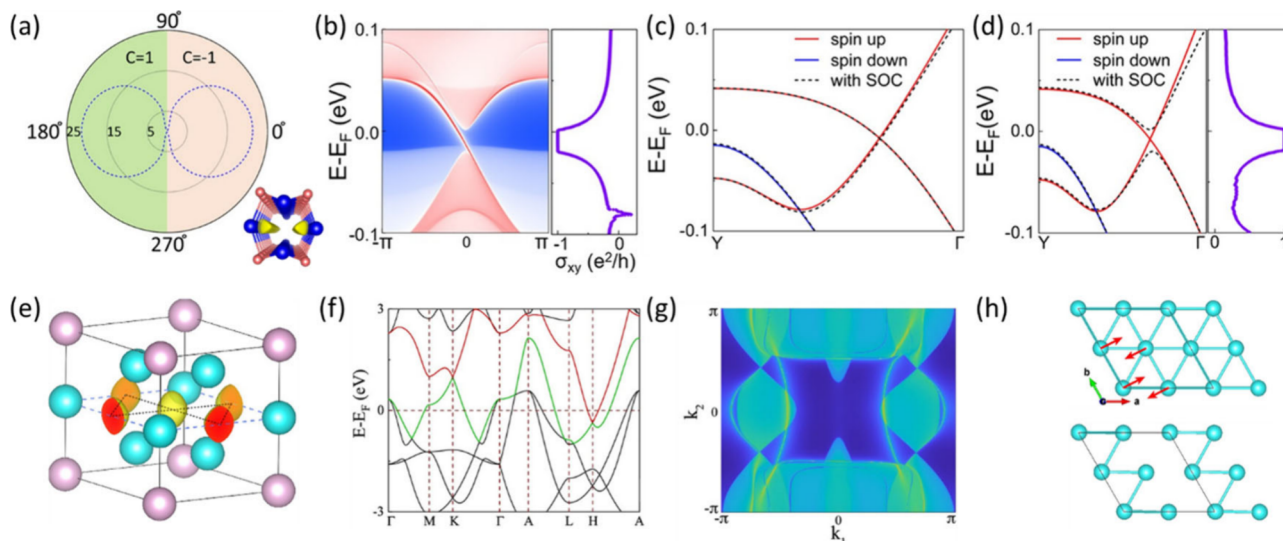


Figure 6. (a) Band gap and Chern number as a function of the magnetization direction characterized by the azimuthal angle, (b) topological edge state and anomalous Hall conductance with the magnetization along the x axis, and band structure without and with spin–orbit coupling with magnetization along the (c) y and (d) x axes for HfBa_4Br_8 . (e) Electron localization function, (f) band structure, (g) topological surface state at an energy of 0.4 eV, and (h) pristine structure (upper panel) and CDW phase (bottom panel) at 110 GPa for Li_5Si . The arrows in (h) show the vibration of the lowest virtual mode at 110 GPa. (a–d) Reproduced from ref 49. Copyright 2023 American Chemical Society. (e–h) Reproduced from ref 4. Copyright 2022 American Chemical Society.

As shown in Figure 4a and 4b, GdI_2 is spin polarized with a band gap of 0.589 eV. Two valleys exist at the K and K' points of the valence band. The spin–orbital coupling lifts the degeneracy between them, yielding a spontaneous valley polarization of 149 meV. Such valley splitting is much larger than that in other reported ferrovalley materials (15–107 meV) and is equivalent to applying a huge magnetic field of \sim 1000 T.⁴¹ This valley splitting is sufficient to overcome the thermal noise at room temperature.⁴⁴ Furthermore, the Berry curvature simulation of GdI_2 shows two sizable valleys with opposite signs with different magnitudes (Figure 4c). With a nonzero out-of-plane Berry curvature, the Bloch electrons in GdI_2 acquire an anomalous Hall velocity under an in-plane longitudinal electric field. Thus, with proper hole doping, when the spin-polarized holes flow through the sample under an external electric field, the holes will accumulate on the boundary and generate a charged Hall current that can be detected by a voltage (Figure 4d). The valley pseudospin can be selectively manipulated and read out by an electric measurement. Such properties are promising for valleytronics, such as data storage.

3.2.2. Inducing Ferromagnetism by a Charge Density Wave. Here, we present a coexistence of CDW and ferromagnetism in the T-phase monolayer LaBr_2 .⁴⁵ T-phase LaBr_2 is dynamically unstable and undergoes a 2×1 reconstruction to a stable T' phase. As shown in Figure 5a–c, the T phase is nonmagnetic and metallic. The La ions in the T phase are octahedrally coordinated, splitting the 5-fold-degenerate d orbitals into doubly degenerate e_g and triply degenerate t_{2g} states. The 3-fold t_{2g} states span from -0.88 to 2.67 eV. The $5d^1$ electrons from La partially occupy such wide bands and are not subject to spin polarization.

The 2×1 CDW distortions in the T'-phase LaBr_2 lead to chemical bonding among La ions, yielding a splitting of t_{2g} orbitals into bonding, nonbonding, and antibonding states. This can be seen from the crystal orbital Hamilton population (COHP) analysis. As shown in Figure 5b, $-\text{COHP}$ values are

positive (bonding), negligible (nonbonding), and negative (antibonding) in the energy ranges of around -0.5 to 0.5 eV, 0.8 to 1.7 eV, and 1.7 to 3.0 eV, respectively. The three-center bonding among the La ions is further confirmed by crystal orbital bond index (COBI) analysis. The high integrated COBI of 0.097 for the three La ions is comparable with that (0.099) of the multicenter bonds in GeTe.⁴⁶ Interestingly, the bonding states are well isolated from the nonbonding states. A similar transition from wide bands to well-separated states has been shown in simple metals by strong compression, yielding the formation of AEs.⁴⁷ The MLWF for the bonding states (lower inset in Figure 5b) further confirms the three-center bonding. Thus, we propose the formation of electride states as the mechanism for the 2×1 CDW distortions in the T'-phase LaBr_2 . This can be further confirmed by the uniformly distributed excess electrons on the La ions in T-phase LaBr_2 (Figure 5a) while the excess electrons are localized in the interstitial region between the La atoms in the T'-phase LaBr_2 (Figure 5b). And the spin density of the T'- LaBr_2 confirms the main contribution from the AEs to the magnetic moments (Figure 5c). Further study reveals that the atomic-orbital-free magnetic AEs possess the dual localized and extended nature and direct exchange coupling from the overlap of the wave functions.² This exotic system provides an exciting platform for exploring new physics and advanced applications for 2D ferromagnetism, CDWs, and spintronic devices.

3.2.3. Topological Properties of 2D Kagome Electrides. Magnetic topological states and phase transitions are promising for spintronic applications. However, reports on magnetic topological phase transitions in electrides are rare. Here, we introduce two ferromagnetic electrenes, HfBa_4Br_8 and HfBa_4Cl_8 , whose magnetic and topological properties are significantly influenced by AE.⁴⁸ The ground state of HfBa_4Br_8 exhibits ferromagnetism with the magnetic moment along the x direction, disrupting the M_y symmetry and opening a band gap at the Weyl point. This leads to the emergence of the quantum anomalous Hall effect (QAHE) with a Chern number

of -1 (Figure 6a). The topological edge state and anomalous Hall conductance are shown in Figure 6b. Additionally, the low MAE facilitates easy in-plane magnetization rotation under the external magnetic fields. Rotation of magnetization to the y -axis maintains mirror symmetry M_y and closes the band gap at the Weyl point, resulting in a Weyl half-semimetal (WHS) state (Figure 6c).⁴⁹ Further rotation to the $-x$ axis induces a QAHE state with an opposite Chern number (Figure 6d). Consequently, the WHS state acts as the critical state between the two QAHE states, periodically modulating the band gaps (Figure 6a). Our exploration of magnetic topological phase transitions in electrides offers a promising platform for advancements in spintronics research.

Dirac cones, van Hove singularities, and flat bands within an ideal Kagome lattice render it promising for investigating novel physical phenomena. However, the intricate 3D structure and multiorder electron hopping in realistic Kagome materials pose significant challenges. We introduce an innovative approach to generate Kagome energy bands within non-Kagome materials by AE, forming a 2D Kagome lattice (Figure 6e), termed 2D Kagome electrides, exemplified by Li_5Si and Li_5Sn .⁴ The band structure exhibits van Hove singularities at the M/L points, Dirac cones at the K/H point, and a flat band at approximately -1.5 eV, characteristic of an ideal Kagome lattice (Figure 6f). Furthermore, the topological nature of these materials is confirmed by the presence of time-reversal pairs of Fermi arcs at approximately 0.4 eV above E_F (Figure 6g). Besides, a CDW phase transition occurs at 110 GPa because of strong Fermi nesting (Figure 6h).

4. POTENTIAL APPLICATIONS OF VDW ELECTRIDES

Given the unique physical and chemical properties of vdw electrides, they hold many potential applications in the fields of new energy, superconductivity, and spintronics. In this section, we demonstrate four examples of the potential applications of vdw electrides.

4.1. K-Ion Battery

The excess interstitial AEs in vdw electrides present a promising opportunity to develop electrode materials, especially for rechargeable metal-ion batteries. Our work shows a remarkable AE-driven high alkali metal ion storage capacity of a 2D electride, $[\text{Sc}_3\text{Si}_2]^{1+} \cdot (1\text{e}^-)$.⁵⁰ Notably, its potassium-ion (K-ion) specific capacity can reach up to 1497 mA·h·g⁻¹, surpassing all previously reported 2D material-based anodes for K-ion batteries. The AEs in $[\text{Sc}_3\text{Si}_2]^{1+} \cdot (1\text{e}^-)$ are crucial for this high capacity as they can drift and balance the charge on metal cations, playing a vital role in stabilizing metal-ion adsorption and enhancing multilayer-ion adsorption. This AE-driven storage mechanism opens new avenues for designing electrode materials with unprecedented storage capacities.

4.2. Thermoelectricity

High “density of scatterings” and low carrier mobility in conventional 2D materials limit their thermoelectric applications. However, the loosely bound electrons with a longer carrier–lattice distance in electrenes will undergo a weaker lattice perturbation, resulting in a higher mobility. Thus, we systematically study the effect of loosely bound electrons, electron–phonon interaction, and spin–orbital interaction on the thermoelectric properties of an electrene, HfI_2 . We found that the larger hole relaxation time of HfI_2 results in a high p-type electrical conductivity and power factor compared with n-type ones. The spin–orbital interaction splits the spin-

degenerate bands near the Fermi level, inducing the decrease in the band gap and slightly increase in electrical conductivity. The electron–phonon interaction also affects the phonon transport under n-type doping, which decreases the lattice thermal conductivity by 16%. Overall, our high-fidelity calculations show a maximum ZT value (1.12) of HfI_2 at 1200 K under p-type doping.⁵¹ Such a result demonstrates the effect of the interaction between anion electrons in vdw electrides with phonons and orbitals on the thermoelectric behavior, providing guidelines for the further design of high-performance 2D thermoelectric devices.

4.3. Superconductor

The Kagome electride Li_5Si emerges as the first reported silicon compound superconductor, exhibiting a low transition temperature of about 1.1 K under ambient pressure. Under 100 GPa, its Curie temperature increases to 7.2 K, which is attributed to the phonon softening due to strong Fermi nesting and the hybridization of Li-s and Si-p orbitals, which strongly couple with phonons. Under 110 GPa, the pristine structure is highly unstable with a softening acoustic phonon mode at the M point. Through vibration mode analysis, reconstructed dimerized zigzag chains are observed (Figure 6h). This yields a CDW phase akin to the T'-phase LaBr_2 . Its T_c is 10.5 K, which is promising as a superconductor.

4.4. Spin–Orbit Torque Memory

The technique of conventional ferromagnet–heavy-metal spin–orbit torque (SOT) offers significant potential for enhancing the efficiency of magnetic memories. However, it faces fundamental limitations, including hunting effects from the metallic layer, broken symmetry for enabling antidamping switching, spin scattering caused by interfacial defects, and sensitivity to stray magnetic fields. Due to the unique intralayer FM and interlayer AFM feature of the bilayer LaBr_2 , it can be used for spin–orbit torque memory devices by addressing the above issues in conventional SOT memory devices. By performing density functional theory and macrospin simulations, we find that electride-based vdw SOT devices exhibit a remarkably low critical current density of approximately 10 MA/cm² and rapid field-free magnetization switching in 250 ps. This indicates excellent writing performance with extremely low energy consumption. Moreover, the device shows a high tunnel magnetoresistance ratio of up to 4250% . The superior write and read performances originate from the unique magnetic interactions in LaBr_2 and the proximity effect from the WTe_2 substrate.

5. CHALLENGES AND PERSPECTIVES

Research on vdw electrides is still in its infancy. Despite recent progress in uncovering the emergent properties of vdw electrides, there remains significant room for exploration. Many topics, such as their optical, mechanical, and piezoelectric properties and their potential applications as catalysts, electron emitters, and reducing agents, have yet to be fully explored in this Account.^{17,52} While we will not cover all of these aspects here, we outline current challenges and several particularly intriguing directions for future research based on the intrinsic properties of vdw electrides.

- a. The chemical reactivity of vdw electrides poses significant challenges for practical applications.⁵³ One solution is to identify stable electrides with excellent chemical and thermal stability in air and water at room

- temperature, such as by forming passivation layers on their surfaces.⁵⁴ Extrinsic methods, such as advanced encapsulation techniques, can prevent the direct exposure of electrides to air.⁵⁵ However, more general and efficient methods need to be discovered to address these stability issues comprehensively.
- b. The number of identified vdW electrides is much less than for other 2D materials. A possible solution is using machine learning (ML) technology. ML and big data have shown their capability to revolutionize the material field as powerful tools for accelerating the identification and development of new materials. Current ML models such as large language models, generative models, and interatomic potentials, have achieved significant success in organic molecule design, catalysis, drug development, etc.⁵⁵ It is foreseeable that ML will also advance the field of electrides by generating new materials, identifying electrides with specific functions for particular applications, providing deeper insights into these materials, and optimizing them for desirable properties.⁵⁶
- c. Beside ferroic properties such as ferromagnetism and ferrovalleys, ferroelectric and ferroelastic electrides have not yet been reported. Theoretically, the AEs and cations can form dipole moments and even collectively align along one direction. Because these AEs are loosely bonded to ions, they could be more easily switched, resulting in a much lower energy barrier for switching electric polarization. Exploring this possibility could open new avenues for developing advanced ferroic materials.
- d. Besides layered materials, vdW materials also include one-dimensional (1D) nanotubes and zero-dimensional (0D) clusters, which are not covered in this Account. These systems can exhibit intriguing properties, such as Majorana bound states in 1D systems. And interesting topological vdW electrides composed of nanotubes have already been reported.⁵⁷ A systematic high-throughput screening of vdW electrides in 1D nanotubes or 0D clusters would also be highly interesting.
- e. With a low work function and high electron density, electrides are highly promising as catalysts. They can form negatively charged active sites that activate molecules such as N₂, H₂, CO, CO₂, and NH₃ through electron injection into their unoccupied orbitals.²⁷ vdW electrides might offer even greater advantages due to their large surface area-to-volume ratio and ease of integration with other materials such as heterostructures.
- f. vdW materials can be tuned using various geometric methods, including forming heterostructures, twisting, and sliding, creating a vast search space for achieving novel properties or designing new materials. The unique AEs in vdW electrides make these strategies particularly promising for developing new electride-based functional materials. For example, a class of quasi-bonds exhibiting characteristics of both ordinary chemical bonds and vdW interactions were reported in heterostructures combining vdW electrides with conventional 2D materials.⁵⁸ Besides, geometric control allows the tuning of wave function of AEs, resulting in various methods of electron confinement. This could lead to new quantum phenomena and new applications. These findings suggest that such innovative approaches could lead to

the discovery of numerous new materials with advanced functionalities.

■ AUTHOR INFORMATION

Corresponding Author

Lei Shen – Department of Mechanical Engineering, National University of Singapore, Singapore 117575, Singapore; National University of Singapore (Chongqing) Research Institute, Chongqing 401123, China;  orcid.org/0000-0001-6198-5753; Email: shenlei@nus.edu.sg

Authors

Jun Zhou – Institute of Materials Research and Engineering (IMRE), Agency for Science, Technology and Research (A*STAR), Singapore 138634, Republic of Singapore;  orcid.org/0000-0002-5505-7616

Jing-Yang You – Department of Physics, National University of Singapore, Singapore 117551, Singapore;  orcid.org/0000-0003-4559-6592

Yi-Ming Zhao – Department of Mechanical Engineering, National University of Singapore, Singapore 117575, Singapore;  orcid.org/0000-0002-3921-1900

Yuan Ping Feng – Department of Physics, National University of Singapore, Singapore 117551, Singapore;  orcid.org/0000-0003-2190-2284

Complete contact information is available at:
<https://pubs.acs.org/10.1021/acs.accounts.4c00394>

Notes

The authors declare no competing financial interest.

Biographies

Jun Zhou obtained a Ph.D. in physics from National University of Singapore. He is currently a senior scientist at Institute of Materials Research and Engineering (IMRE), Agency for Science, Technology and Research (A*STAR), Singapore.

Jing-Yang You holds a Ph.D. in physics from University of Chinese Academy of Sciences. He is currently a research fellow in the Department of Chemistry at National University of Singapore.

Yi-Ming Zhao obtained a B.S. from University of Chinese Academy of Sciences. Currently, he is a Ph.D. candidate in the Department of Mechanical Engineering at National University of Singapore.

Yuan Ping Feng has a Ph.D. in physics from the Illinois Institute of Technology. He now is an emeritus professor at National University of Singapore.

Lei Shen has a Ph.D. in physics from National University of Singapore. He is currently a senior lecturer of mechanical engineering and an associate of the engineering science programme at National University of Singapore.

■ ACKNOWLEDGMENTS

This work is supported by the Singapore Ministry of Education (MOE) (no. MOE-T2EP50123-0012). The authors acknowledge the National Supercomputing Centre Singapore (NSCC) for providing computing resources.

■ REFERENCES

- (1) Zhou, J.; Shen, L.; Yang, M.; Cheng, H.; Kong, W.; Feng, Y. P. Discovery of Hidden Classes of Layered Electrides by Extensive High-

- Throughput Material Screening. *Chem. Mater.* **2019**, *31* (6), 1860–1868.
- (2) Zhou, J.; Feng, Y. P.; Shen, L. Atomic-orbital-free intrinsic ferromagnetism in electrenes. *Phys. Rev. B* **2020**, *102* (18), 180407R.
- (3) Cheng, H.-X.; Zhou, J.; Ji, W.; Zhang, Y.-N.; Feng, Y.-P. Two-dimensional intrinsic ferrovalley GdI_2 with large valley polarization. *Phys. Rev. B* **2021**, *103* (12), 125121.
- (4) You, J. Y.; Gu, B.; Su, G.; Feng, Y. P. Emergent Kagome Electrides. *J. Am. Chem. Soc.* **2022**, *144* (12), 5527–5534.
- (5) Dye, J. L. Anionic electrons in electrides. *Nature* **1993**, *365* (6441), 10–11.
- (6) Kraus, C. A. Solutions of metals in non-metallic solvents; I. general properties of solutions of metals in liquid ammonia. *J. Am. Chem. Soc.* **1907**, *29* (11), 1557–1571.
- (7) Ellaboudy, A.; Dye, J. L.; Smith, P. B. Cesium 18-Crown-6 Compounds. A Crystalline Ceside and a Crystalline Electride. *J. Am. Chem. Soc.* **1983**, *105* (21), 6490–6491.
- (8) Wagner, M. J.; Huang, R. H.; Eglin, J. L.; Dye, J. L. An electride with a large six-electron ring. *Nature* **1994**, *368* (6473), 726–729.
- (9) Issa, D.; Dye, J. L. Synthesis of cesium 18-crown-6: the first single-crystal electride? *J. Am. Chem. Soc.* **1982**, *104* (13), 3781–3782.
- (10) Matsuishi, S.; Toda, Y.; Miyakawa, M.; Hayashi, K.; Kamiya, T.; Hirano, M.; Tanaka, I.; Hosono, H. High-density electron anions in a nanoporous single crystal: $[\text{Ca}_{24}\text{Al}_{28}\text{O}_{64}]^{4+}(4\text{e}^-)$. *Science* **2003**, *301* (5633), 626–629.
- (11) Kim, K.-B.; Kikuchi, M.; Miyakawa, M.; Yanagi, H.; Kamiya, T.; Hirano, M.; Hosono, H. Photoelectron spectroscopic study of C12A7 : e^- and Alq_3 interface: The formation of a low electron-injection barrier. *J. Phys. Chem. C* **2007**, *111* (24), 8403–8406.
- (12) Toda, Y.; Kim, S. W.; Hayashi, K.; Hirano, M.; Kamiya, T.; Hosono, H.; Haraguchi, T.; Yasuda, H. Intense thermal field electron emission from room-temperature stable electride. *Appl. Phys. Lett.* **2005**, *87* (25), 203401.
- (13) Meng, W.; Zhang, X.; Liu, Y.; Dai, X.; Liu, G.; Gu, Y.; Kenny, E. P.; Kou, L. Multifold Fermions and Fermi Arcs Boosted Catalysis in Nanoporous Electride $12\text{CaO}\cdot7\text{Al}_2\text{O}_3$. *Adv. Sci.* **2023**, *10* (6), e2205940.
- (14) Feng, Y. P.; Shen, L.; Yang, M.; Wang, A.; Zeng, M.; Wu, Q.; Chintalapati, S.; Chang, C.-R. Prospects of spintronics based on 2D materials. *Wiley Interdiscip. Rev. Comput. Mol. Sci.* **2017**, *7* (5), e1313.
- (15) Shen, L.; Zhou, J.; Yang, T.; Yang, M.; Feng, Y. P. High-Throughput Computational Discovery and Intelligent Design of Two-Dimensional Functional Materials for Various Applications. *Accounts of Materials Research* **2022**, *3* (6), 572–583.
- (16) Lee, K.; Kim, S. W.; Toda, Y.; Matsuishi, S.; Hosono, H. Dicalcium nitride as a two-dimensional electride with an anionic electron layer. *Nature* **2013**, *494* (7437), 336–340.
- (17) Druffel, D. L.; Woerner, A. H.; Kuntz, K. L.; Pawlik, J. T.; Warren, S. C. Electrons on the surface of 2D materials: from layered electrides to 2D electrenes. *J. Mater. Chem. C* **2017**, *5* (43), 11196–11213.
- (18) Zhang, Y.; Wang, H.; Wang, Y.; Zhang, L.; Ma, Y. Computer-Assisted Inverse Design of Inorganic Electrides. *Phys. Rev. X* **2017**, *7* (1), 019903.
- (19) Tada, T.; Takemoto, S.; Matsuishi, S.; Hosono, H. High-throughput ab initio screening for two-dimensional electride materials. *Inorg. Chem.* **2014**, *53* (19), 10347–58.
- (20) Inoshita, T.; Takemoto, S.; Tada, T.; Hosono, H. Surface electron states on the quasi-two-dimensional excess-electron compounds Ca_2N and Y_2C . *Phys. Rev. B* **2017**, *95* (16), 165430.
- (21) Wang, J.; Hanzawa, K.; Hiramatsu, H.; Kim, J.; Umezawa, N.; Iwanaka, K.; Tada, T.; Hosono, H. Exploration of Stable Strontium Phosphide-Based Electrides: Theoretical Structure Prediction and Experimental Validation. *J. Am. Chem. Soc.* **2017**, *139* (44), 15668–15680.
- (22) Jain, A.; Ong, S. P.; Hautier, G.; Chen, W.; Richards, W. D.; Dacek, S.; Cholia, S.; Gunter, D.; Skinner, D.; Ceder, G.; Persson, K. A. Commentary: The Materials Project: A materials genome approach to accelerating materials innovation. *APL Mater.* **2013**, *1* (1), 011002.
- (23) Ashton, M.; Paul, J.; Sinnott, S. B.; Hennig, R. G. Topology-Scaling Identification of Layered Solids and Stable Exfoliated 2D Materials. *Phys. Rev. Lett.* **2017**, *118* (10), 106101.
- (24) Wang, Z.; Chu, I.-H.; Zhou, F.; Ong, S. P. Electronic Structure Descriptor for the Discovery of Narrow-Band Red-Emitting Phosphors. *Chem. Mater.* **2016**, *28* (11), 4024–4031.
- (25) Hellenbrandt, M. The Inorganic Crystal Structure Database (ICSD)—Present and Future. *Crystallogr. Rev.* **2004**, *10* (1), 17–22.
- (26) Huang, B.; Clark, G.; Navarro-Moratalla, E.; Klein, D. R.; Cheng, R.; Seyler, K. L.; Zhong, D.; Schmidgall, E.; McGuire, M. A.; Cobden, D. H.; Yao, W.; Xiao, D.; Jarillo-Herrero, P.; Xu, X. Layer-dependent ferromagnetism in a van der Waals crystal down to the monolayer limit. *Nature* **2017**, *546* (7657), 270–273.
- (27) Zhang, X.; Meng, W.; Liu, Y.; Dai, X.; Liu, G.; Kou, L. Magnetic Electrides: High-Throughput Material Screening, Intriguing Properties, and Applications. *J. Am. Chem. Soc.* **2023**, *145* (9), 5523–5535.
- (28) Stoner, E. C. Collective electron ferronmagnetism. *Proc. R. Soc. London, Ser. A* **1938**, *165* (922), 372–414.
- (29) Solovyev, I. V.; Pchelkina, Z. V.; Mazurenko, V. V. Magnetism of sodium superoxide. *CrystEngComm* **2014**, *16* (4), 522–531.
- (30) Mostofi, A. A.; Yates, J. R.; Lee, Y.-S.; Souza, I.; Vanderbilt, D.; Marzari, N. wannier90: A tool for obtaining maximally-localised Wannier functions. *Comput. Phys. Commun.* **2008**, *178* (9), 685–699.
- (31) Anderson, P. W. New Approach to the Theory of Superexchange Interactions. *Phys. Rev.* **1959**, *115* (1), 2–13.
- (32) Ising, E. Beitrag zur Theorie des Ferromagnetismus. *Z. Phys.* **1925**, *31* (1), 253–258.
- (33) Heisenberg, W. On the theory of ferromagnetism. *Z. Phys.* **1928**, *49* (9), 619–636.
- (34) Zhou, J.; Song, X.; Yang, M.; Chai, J.; Wong, N. L. M.; Shen, L.; Wang, S.; Feng, Y. P. A first principles study of uniaxial strain-stabilized long-range ferromagnetic ordering in electrenes. *J. Mater. Chem. C* **2021**, *9* (46), 16576–16580.
- (35) Jiang, S.; Li, L.; Wang, Z.; Mak, K. F.; Shan, J. Controlling magnetism in 2D CrI_3 by electrostatic doping. *Nat. Nanotechnol.* **2018**, *13* (7), 549–553.
- (36) He, J.; Chen, Y.; Wang, Z.; Yang, M.; Yang, T.; Shen, L.; Xu, X.; Jiang, Y.; Chai, J.; Wong, L. M.; Wang, S.; Feng, Y. P.; Zhou, J. Formation of magnetic anionic electrons by hole doping. *J. Mater. Chem. C* **2022**, *10* (19), 7674–7679.
- (37) Zhang, L.; Yang, Z.; Gong, T.; Pan, R.; Wang, H.; Guo, Z.; Zhang, H.; Fu, X. Recent advances in emerging Janus two-dimensional materials: from fundamental physics to device applications. *J. Mater. Chem. A* **2020**, *8* (18), 8813–8830.
- (38) Chen, Y.; He, J.; Wang, S.; Feng, Y. P.; Zhou, J. Tuning the magnetic and electronic properties of two-dimensional electrides by forming cationic Janus compounds. *J. Alloys Compd.* **2023**, *930*, 167417.
- (39) Grüner, G. The dynamics of charge-density waves. *Rev. Mod. Phys.* **1988**, *60* (4), 1129.
- (40) Sham, L. J.; Allen, S. J.; Kamgar, A.; Tsui, D. C. Valley-Valley Splitting in Inversion Layers on a High-Index Surface of Silicon. *Phys. Rev. Lett.* **1978**, *40* (7), 472–475.
- (41) Tong, W.-Y.; Gong, S.-J.; Wan, X.; Duan, C.-G. Concepts of ferrovalley material and anomalous valley Hall effect. *Nat. commun.* **2016**, *7* (1), 13612.
- (42) Eick, H. A. The lanthanoid (II) halides: still a veritable gold mine. *J. Less Common. Met.* **1987**, *127*, 7–17.
- (43) Wang, B.; Zhang, X.; Zhang, Y.; Yuan, S.; Guo, Y.; Dong, S.; Wang, J. Prediction of a two-dimensional high-TC f-electron ferromagnetic semiconductor. *Mater. Horiz.* **2020**, *7* (6), 1623–1630.
- (44) Vitale, S. A.; Nezich, D.; Varghese, J. O.; Kim, P.; Gedik, N.; Jarillo-Herrero, P.; Xiao, D.; Rothschild, M. Valleytronics: Opportunities, Challenges, and Paths Forward. *Small* **2018**, *14* (38), 1801483.
- (45) Zhou, J.; Wang, Z.; Wang, S.; Feng, Y. P.; Yang, M.; Shen, L. Coexistence of ferromagnetism and charge density waves in monolayer LaBr_2 . *Nanoscale Horiz.* **2023**, *8* (8), 1054–1061.

- (46) Hempelmann, J.; Muller, P. C.; Ertural, C.; Dronskowski, R. The Orbital Origins of Chemical Bonding in Ge-Sb-Te Phase-Change Materials. *Angew. Chem., Int. Ed. Engl.* **2022**, *61* (17), e202115778.
- (47) Rousseau, B.; Ashcroft, N. W. Interstitial electronic localization. *Phys. Rev. Lett.* **2008**, *101* (4), 046407.
- (48) Zhang, Z.; You, J.-Y. Tunable Topological Phases in Two-Dimensional Electrides. *ACS Mater. Lett.* **2023**, *5* (7), 1870–1875.
- (49) You, J.-Y.; Chen, C.; Zhang, Z.; Sheng, X.-L.; Yang, S. A.; Su, G. Two-dimensional Weyl half-semimetal and tunable quantum anomalous Hall effect. *Phys. Rev. B* **2019**, *100* (6), 064408.
- (50) Chen, Y.; Qin, H.; Zhou, J.; Yang, T.; Sun, B.; Ni, Y.; Wang, H.; Redfern, S. A. T.; Miao, M.; Lin, H. Q.; Feng, Y. P. Unveiling Interstitial Anionic Electron-Driven Ultrahigh K-Ion Storage Capacity in a Novel Two-Dimensional Electride Exemplified by Sc_3Si_2 . *J. Phys. Chem. Lett.* **2022**, *13* (32), 7439–7447.
- (51) Zhao, Y.-M.; Wang, Z.; Zhou, J.; Zhang, C.; Shin, S.; Shen, L. Effects of loosely bound electrons and electron-phonon interaction on thermoelectric properties of electrenes. *J. Mater. Chem. C* **2024**, DOI: 10.1039/D4TC01927J.
- (52) Wu, Y.; Abdelwahab, I.; Kwon, K. C.; Verzhbitskiy, I.; Wang, L.; Liew, W. H.; Yao, K.; Eda, G.; Loh, K. P.; Shen, L.; Quek, S. Y. Data-driven discovery of high performance layered van der Waals piezoelectric NbOI_2 . *Nat. Commun.* **2022**, *13* (1), 1884.
- (53) Zhao, S.; Li, Z.; Yang, J. Obtaining two-dimensional electron gas in free space without resorting to electron doping: an electride based design. *J. Am. Chem. Soc.* **2014**, *136* (38), 13313–8.
- (54) Kang, S. H.; Thapa, D.; Regmi, B.; Ren, S.; Kim, Y. M.; Kim, S. G.; Kim, S. W. Chemically Stable Low-Dimensional Electrides in Transition Metal-Rich Monochalcogenides: Theoretical and Experimental Explorations. *J. Am. Chem. Soc.* **2022**, *144* (10), 4496–4506.
- (55) Choudhary, K.; DeCost, B.; Chen, C.; Jain, A.; Tavazza, F.; Cohn, R.; Park, C. W.; Choudhary, A.; Agrawal, A.; Billinge, S. J. L.; Holm, E.; Ong, S. P.; Wolverton, C. Recent advances and applications of deep learning methods in materials science. *npj Comput. Mater.* **2022**, *8* (1), 59.
- (56) Wang, Z.; Gong, Y.; Evans, M. L.; Yan, Y.; Wang, S.; Miao, N.; Zheng, R.; Rignanese, G. M.; Wang, J. Machine Learning-Accelerated Discovery of A_2BC_2 Ternary Electrides with Diverse Anionic Electron Densities. *J. Am. Chem. Soc.* **2023**, *145* (48), 26412–26424.
- (57) Wang, J.; Sui, X.; Gao, S.; Duan, W.; Liu, F.; Huang, B. Anomalous Dirac Plasmons in 1D Topological Electrides. *Phys. Rev. Lett.* **2019**, *123* (20), 206402.
- (58) Woomer, A. H.; Druffel, D. L.; Sundberg, J. D.; Pawlik, J. T.; Warren, S. C. Bonding in 2D Donor-Acceptor Heterostructures. *J. Am. Chem. Soc.* **2019**, *141* (26), 10300–10308.